NEW MOTHER WAVELET FOR PATTERN DETECTION IN IR IMAGE

M. Ali Mirzaei[1], *Sugeng Prianto*[2], *Jean-Rémy Chardonnet*[1], *Christian Père*[1], *Frédéric Mérienne*[1]

[1]Arts et Metiers ParisTech, CNRS, Le2i, France, [2]University of Brawijaya,Indonesia

ABSTRACT

The paper presents a new mother wavelet adapted from a specific pattern. Wavelet multi-resolution analysis uses this wavelet to detect the position of the pattern in an Infra-Red (IR) signal under scale variation and the presence of noise. IR signal is extracted from IR image sequence recorded by an IR camera, Time of Flight (TOF) sensor configuration. The maximum correlation between the pattern and the signal of interest will be used as a criterion to define the mother wavelet. The proposed mother wavelet were tested and verified under the scale variation and the presence of noise. The experimental tests and performance analysis show promising results for both scale variation and noisy signal. 90% accuracy for the proposed wavelet under intensive noisy condition (50% of the signal amplitude) is guaranteed and high precision is expected under real condition.

Index Terms— IR image, adapted mother wavelet, pattern detection, multi-resolution analysis

1. INTRODUCTION

Wavelet transform introduces a method that cuts up signals into different frequency components, and then studies each component with a resolution matched to its scale [1]. One of the advantages of wavelet over Fourier analysis is the flexibility in the "shape" and the "form" of the analyzer. However, the difficult task of choosing or designing a suitable mother wavelet for a specific signal comes with the flexibility.

Applying Multi-Resolution Decomposition (MRD) to a signal in the presence of noise using a matched wavelet [2] would generate a sharper peak in time-scale space as compared to standard non-matched wavelets. Wavelet design methods developed up to now do not specifically address the need for maximizing correlation with the signal decomposition.

Daubechies [3] proposed a technique for finding orthonormal wavelet bases with compact support and over limited number of scales, totally independent of the signal being analyzed. Jorgensen et al. [4] have developed and extended a technique for finding the optimal orthonormal wavelet basis for representing a specified signal within a finite number of scales. Mallat [5] developed non-orthonormal wavelet bases for MRD in such a way that some error cost function is minimized. This approach employs a set of mother wavelets and combined them to build a new wavelet. Aldroubi [6] matched a wavelet basis to a desired signal by both projecting the desired signal onto an existing wavelet basis, and transforming the wavelet basis under certain conditions such that it optimizes the error norm between the desired signal and the new basis.

Gait analysis [7], human locomotion perception and interpretation, is an important task in many automotive vision systems and plays a key role in designing a gesture-based human-machine interface (HMI) [8].

The initial step of most of the gait recognition algorithms is human silhouette extraction [9]. Many gait recognition systems use CCD sensors similar to one existing in RGB cameras. However, it is very likely that some part of the human body or clothing has colors similar to the background. Human silhouette extraction usually fails on this part. Moreover, the existence of shadows and poor lighting conditions is another problem [10]. To avoid these problems and other environmental effects, Infra-Red (IR) sensor is used in a carefully arranged laser projector-IR sensor configuration.

Preis et al. [11] presented an approach for gait recognition with Microsoft Kinect and an integrated depth sensor allowing for skeleton detection and gait tracking in real-time based on nave Bayesian filter. Stone [12] [13] proposed a webcam-Kinect set-up and local maximum and minimum as feature to detect left and right gait. Iwashita [14] proposed multiple thresholds to detect the gait with scale variation.

Although, gait pattern recognition is a complicated task and requires better detection approaches. The main problem is the variation of the signal amplitude with the alternation of the distance between the target (human body) and the sensor.

The paper proposed a new method based on wavelet Multi-Resolution Analysis (MRA) and pattern localization to solve this problem. A mother wavelet will be adapted directly from gait pattern in the proposed approach (section 3, 4).

The paper is organized into following sections: Section 2 contains information on how gait signal is extracted from IR images. Optoelectronic setup for image acquisition and TOF theory will be introduced in this section. Section 3 explains the theory and formulation of wavelet MRA for use throughout the paper. We will adapt a mother wavelet to match the amplitude and phase of the pattern in Section 4 by applying matched filter theory to the wavelet decomposition. Section 5

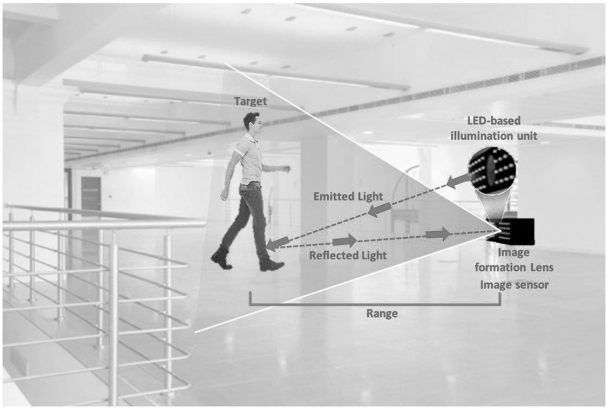

Fig. 1: Typical TOF sensor configuration with an optical device

applies our technique to the signal of interest to demonstrate the performance of the proposed mother wavelet and compare the result with other standard mother wavelets.

2. IR IMAGE ANALYSIS AND SIGNAL EXTRACTION

IR image sequence was captured using TOF during practical experiments. A typical TOF sensor consists in a modulated light source such as laser or LED-based illumination, image sensor (linear or rectangular array of pixels, each capable of detecting the phase of the incoming light) and an ordinary optical device for focusing the reflected light onto the sensor (Fig. 1). The light is modulated on an envelope of square wave which is created by rapidly turning the light source on and off. Distance is measured by the phase of the transmitted light as received at the pixel array. Although pulse waves are employed in practice for modulation, here sinusoidal waves will be discussed for the ease of explanation. Let us assume $s(t) = \sin(2\pi f_m t)$ be the transmitted light where, f_m is the modulation frequency. The reflected light from the target object creates a phase shift ϕ:

$$r(t) = R\sin(2\pi f_m t - \phi) = R\sin(2\pi f_m (t - 2d/c)) \quad (1)$$

Where, R is the amplitude of the reflected light, d is the distance between the sensor and the target object (range in Fig. 1), and c is the speed of light, 3×10^8 m/s. The distance, d, is calculated by $d = c\phi/(4\pi f_m)$. The maximum unambiguous phase delay that can be detected using TOF is a full cycle of the modulation period, which corresponds to an unambiguous range of $c/(2f_m)$. For example, the maximum unambiguous range for $f_m = 50$MHz is 3m. In practice, phase detection can be implemented more efficiently as described in [15]. The reflected laser beam from the target object is recorded by IR sensor and processed to extract and integrate depth information in the image by color (gray scale) coding (Fig. 2.a). Rizon [16] proposed a method to detect the object (e.g., a human body) in the sequence of image stream. Figure 2.b shows

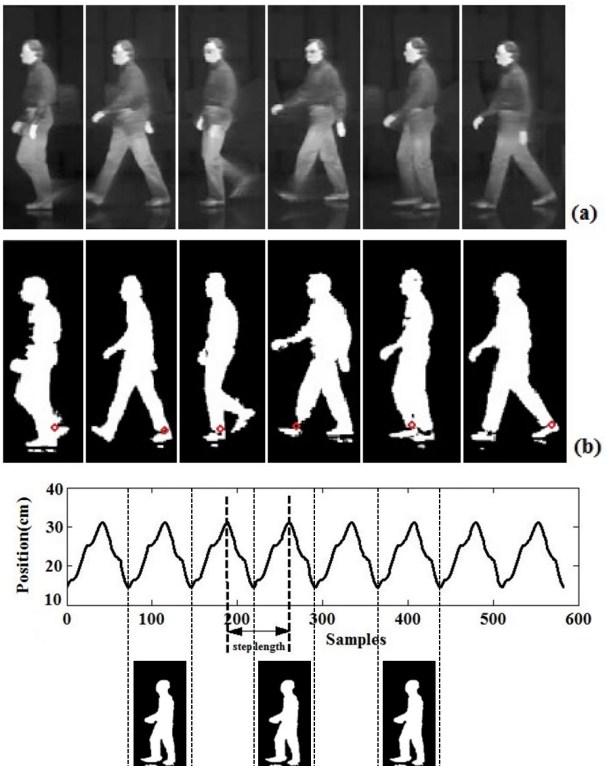

Fig. 3: Walking signal with constant distance from IR sensor

the detected human body in IR image sequence. The position of the red circle is tracked in the sequence and depicted versus time (or sample), which forms the gait (walking) signal. An example of this signal with constant step length is depicted in Fig. 3. When the person walks in parallel with the image plane of the sensor, the amplitude of the signal is quite constant, maximum and minimum of the signal are the same everywhere, because the scale of human body is constant. But, when the person displaces along the z-axis (perpendicular to the image plane and outward) of the sensor the scale changes, the amplitude of the signal varies consequently (Fig. 4) which makes gait pattern detection very difficult with ordinary techniques such as constant threshold and adaptive threshold. Section 3 and 4 will propose a method to detect the pattern with a new mother wavelet.

3. WAVELET MULTI-RESOLUTION ANALYSIS

Wavelet application to multi-resolution signal decomposition has been thoroughly discussed in the literature over the past decades. We will summarize the principle of dyadic MRA and final equations below. A linear space L of $\mathbb{R}$, $L(\mathbb{R})$, is divided into a set of subspaces $\{V_j\}$. By definition, the subspace V_j ($j \in \mathbb{Z}$) should satisfy properties (2), (3) as well.

$$\cdots \subset V_2 \subset V_1 \subset V_0 \subset V_{-1} \subset V_{-2} \subset \cdots \quad (2)$$

$$\bigcap_{j\in\mathbb{Z}} V_j = \{0\}, \bigcup_{j\in\mathbb{Z}} \overline{V_j} = L(\mathbb{R}) \quad (3)$$

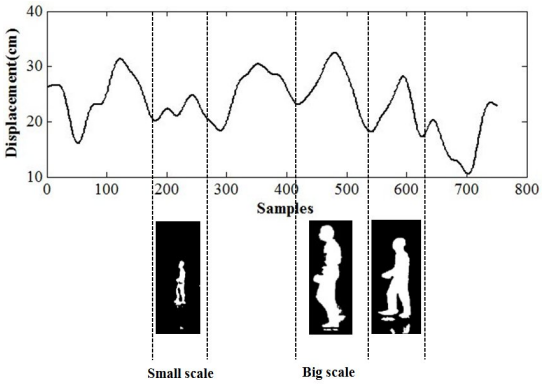

Fig. 4: Walking signal with different scales (different distances from the sensor)

In a MRA a signal (time series), $x(t) \in V_{-1}, V_{-1} \subseteq L(\mathbb{R})$ can be decomposed into linear combination of an infinite series of detail functions, $\{G_0, G_1, \cdots, G_n \cdots\}$, so that

$$x(t) = \sum_{k=0}^{\infty} a_k G_k(t) \tag{4}$$

Where, k is the integer index of the infinite sum and a_k is expansion coefficients. In an orthonormal multiresolution analysis (OMRA) [17], a signal is represented by a sum of a more flexible function called mother wavelet $\psi(t)$, localized both in time and frequency spaces, and scaling function $\varphi(t)$, where

$$\int \psi(t)dt = 0 \tag{5}$$

$$\int \varphi(t)dt = 1 \tag{6}$$

The set $\left\{\psi_{j_1,k_1}(t) = 2^{-j_1/2}\varphi\left(2^{-j_1}t - k_1\right), k_1 \in \mathbb{Z}\right\}$ and $\left\{\phi_{j_2,k_2}(t) = 2^{-j_2/2}\varphi\left(2^{-j_2}t - k_2\right), k_2 \in \mathbb{Z}\right\}$ construct the orthonormal basis for V_j and W_j respectively. Then V_j for instance, can be expressed as, $V_j = \text{span}\{\psi_{j,k}(t), k \in \mathbb{Z}\}$. This type of decompositions is usually based on a scale factor 2, however any scaling factor can be used for this purpose. The decomposition based on scale factor 2 is called dyadic decomposition. The first level decomposition is constructed by projecting $x(t)$ onto two orthogonal subspaces, V_0 and W_0, where $V_{-1} = V_0 \oplus W_0$ is the direct sum operator. The projection produces $x_0(t) \in V_0$, a low resolution approximation of $x(t)$, and $y_0(t) \in W_0$, the detail lost in going from $x(t)$ to $x_0(t)$. The decomposition continues by projecting $x_0(t)$ onto V_1 and W_1 and so on. Note that W_j is the orthogonal complement of spaces V_j and V_{j+1} that can be expressed as:

$$V_{j+1} = V_j \oplus W_j \tag{7}$$

In general,

$$V_j = V_{j_0} \oplus W_{j_0} \oplus \cdots \oplus W_{j-1}, j \succ j_0 \tag{8}$$

And

$$L(\mathbb{R}) = V_0 \oplus W_0 \oplus W_1 \oplus W_2 \oplus W_3 \cdots \tag{9}$$

A signal $x(t)$ is projected onto V_j and W_j using projection equations (10), (11).

$$x_j(t) = \sum_{k=-\infty}^{\infty} d_k^j 2^{-\left(\frac{j}{2}\right)} \psi\left(2^{-j}t - k\right) \tag{10}$$

$$y_j(t) = \sum_{k=-\infty}^{\infty} c_k^j 2^{-\left(\frac{j}{2}\right)} \phi\left(2^{-j}t - k\right) \tag{11}$$

Where, $d_k^j = \langle x_{j-1}(t), \psi_{j,k}\rangle$ and $c_k^j = \langle x_{j-1}(t), \phi_{j,k}\rangle$ are the projection coefficients and $\langle ., .\rangle$ denotes the inner product in L^2. The inner product of two complex functions $u(t)$ and $v(t)$ may be defined on the interval $a \leq x \leq b$ by (12),

$$\langle u(t), v(t)\rangle = \int_a^b u(t)v^*(t)dt \tag{12}$$

The satisfying result comes because of the orthonormal property of the basis. It is important to choose an appropriate set of basis and dual for the signal decomposition. If a particular basis satisfies the orthonormal property for a given signal which we want to deal with, it will be easier to find the expansion coefficients. Fortunately, the coefficients concentrate on some critical values, while others are close to zero. We can drop the small coefficients and use the important values to decrease calculation time and keep more memory space for more important data. For the MRA to be orthonormal, three conditions are required:

1. $\psi_{j,k}$ and $\phi_{j,k}$ must be orthonormal bases of W_j and V_j respectively
2. $W_j \perp W_k$, for $j \neq k$
3. $W_j \perp V_k$,

which leads to the following conditions (13)-(15) on ψ and ϕ accordingly

$$\langle \phi_{j,k}, \phi_{j,m}\rangle = \delta_{k,m} \tag{13}$$

$$\langle \phi_{j,k}, \psi_{j,m}\rangle = 0 \tag{14}$$

$$\langle \psi_{j,k}, \psi_{l,m}\rangle = \delta_{j,l}\delta_{k,m} \tag{15}$$

Since $\phi(t) \in V_0 \subset V_{-1}$ and $\psi(t) \in W_0 \subset V_{-1}$, they can be represented as linear combinations of the basis of V_{-1}.

$$\phi(t) = 2\sum_{k=-\infty}^{\infty} h_k \varphi(2t - k) \tag{16}$$

$$\psi(t) = 2\sum_{k=-\infty}^{\infty} g_k \varphi(2t - k) \tag{17}$$

For orthonormal MRAs, the sequences h_k and g_k in (16) and (17) represent the impulse responses of quadrature mirror filters (QMF) and have the following properties:

$$H(\omega)\overline{H(\omega + \pi)} + G(\omega)\overline{G(\omega + \pi)} = 0 \tag{18}$$

$$|H(\omega)|^2 + |G(\omega)|^2 = 1 \tag{19}$$

Where $H(\omega)$ and $G(\omega)$ are the Fourier transforms of h_k and g_k, respectively, and are therefore both 2π-periodic. Here,

$$g_k = (-1)^{k+1} h_{1-k} \Leftrightarrow G(\omega) = e^{i\omega}\overline{H(\omega+\pi)} \tag{20}$$

Thereby guaranteeing (20) is always satisfied.

4. NEW WAVELET ADAPTATION FROM PATTERN

Using a matched filter bank interpretation of wavelet transforms [18], we propose to design a wavelet that "matches" the signal of interest such that the output of the matched filter bank is maximized. The projection equation for the detail functions, given in (11), is an inner product integral and can be rewritten in the frequency domain by way of Parseval's identity (21)

$$d_k^j = \langle x(t), \psi_{j,k} \rangle = \left\langle X(\omega), \Psi_{j,k}\left(2^j\omega\right)\right\rangle \tag{21}$$

Where $\Psi_{j,k}\left(2^j\omega\right) = 2^{j/2}e^{i2^j\omega k}\Psi\left(2^j\omega\right)$, is the Fourier transform of $\psi_{j,k}(t)$. The energy of d_k^j at a particular scale, j_0, and translation, k_0, is given by its squared magnitude

$$\left|d_{k_0}^{j_0}\right|^2 = \left|\left\langle X(\omega), \Psi_{j_0,k_0}\left(2^{j_0}\omega\right)\right\rangle\right|^2 \tag{22}$$

Applying the Cauchy-Schwarz inequality to the right side of (22) gives

$$\left|\left\langle X(\omega), \Psi_{j_0,k_0}\left(2^{j_0}\omega\right)\right\rangle\right|^2 \leq \langle X(\omega), X(\omega)\rangle \left\langle \Psi_{j_0,k_0}\left(2^{j_0}\omega\right), \Psi_{j_0,k_0}\left(2^{j_0}\omega\right)\right\rangle \tag{23}$$

where the equality holds if and only if

$$X(\omega) = K\Psi_{j_0,k_0}\left(2^{j_0}\omega\right) \tag{24}$$

Both X and Ψ are complex spectra. Therefore, $\left|d_{k_0}^{j_0}\right|^2$ is maximized when the complex frequency spectrum of ψ_{j_0,k_0} is identical to that of $x(t)$. Therefore, we would like to develop a method for matching the complex spectrum of the wavelet to that of the desired signal while maintaining the conditions for an orthonormal MRA. However, because the conditions for orthonormality are on the spectrum amplitude (Poisson summation) only, our solution matches the spectrum amplitudes and group delays independently.

To overcome the difficulty in matching the wavelet spectrum directly to that of the desired signal we must propagate the conditions for an orthonormal MRA [2] from the 2-scale sequence and scaling function to the wavelet. Then calculate the scaling function and 2-scale sequence always guaranteeing that the conditions for an orthonormal MRA are satisfied. For a given function $f(t)$ with compact support and finite energy we may consider the construction of a wavelet for MRA, approximating this function by minimizing the least squares error. Four methods of matching mother wavelet to a pattern will be considered.

4.1. First Method

We want to construct the approximation in the least squares sense of the function f using a finite linear combination of the form $\psi = \sum_{i=1}^{N} \alpha_i \rho_i$. Given the hypotheses on f and $F = \{\rho_i\}_{i=1}^{N}$, a set of continuous or piecewise continuous functions on $[a, b]$, the approximation ψ clearly satisfies the two conditions $\psi \in L^1 \cap L^2$ and $t\psi \in L^1$. This condition reduces to the following linear constraint: $\sum_{i=1}^{N} \alpha_i R_i = 0$ where $R_i = \int_a^b \rho_i(t)dt$. ψ is obtained by solving a linear system.

4.2. Second Method

Since the family F consists in continuous functions on $[a, b]$ we may seek a function ψ continuous on $\mathbb{R}$. $\psi(a) = 0$ and $\psi(b) = 0$ are two additional linear constraints leading to $\sum_{i=1}^{N} \alpha_i \rho_i(a) = 0$ and $\sum_{i=1}^{N} \alpha_i \rho_i(b) = 0$. ψ will be obtained in the same way as in 4.1.

4.3. Third Method

We can use a more direct construction method. We seek the best approximation of f in the least squares sense, within the space of functions orthogonal to constants. If f is continuous over the interval $[a, b]$, satisfying the two additional constraints $\psi(a) = 0$ and $\psi(b) = 0$ leads to seeking a wavelet ψ of the form:

$$\psi = f - \left(\alpha t^2 + \beta t + \gamma\right) \tag{25}$$

4.4. Fourth Method

In practice and for numerical calculations we generally know only one sampling of the function f over the $[a, b]$ interval. We have a finite set of values $\{(t_k, y_k)\}_{k=1,\cdots,k}$ such that: $a \leq t_k \leq b$ and $y_k \approx f(t_k)$. As above, we consider a family $F = \{\rho_i\}_i^N = 1$ linearly independent in $L^2(a, b)$, and we denote by V the span vector space of F. Formulated for this finite set of pairs, the problem is seeking $\alpha = \{\alpha_i\}_{i=1}^{N}$ in $\mathbb{R}^N$ and thus $\psi = \sum_{i=1}^{N} \alpha_i \rho_i$ such that:

$$\sum_{k=1}^{K} \left[\psi(t_k) - y_k\right]^2 = \min_{\beta \in \mathbb{R}^N} \left\{ \sum_{k=1}^{K} \left[v_\beta(t_k) - y_k\right]^2 \text{ such that } \int_a^b v_\beta(t)dt = 0 \right\} \tag{26}$$

Where for β in $\mathbb{R}^N$, $v_\beta = \sum_{i=1}^{N} \beta_i \rho_i$. The last method is applied to our problem to match a mother wavelet to the pattern. We apply the method to the pattern shown in Fig. 5 will calculate mother wavelet (Fig. 6). This mother wavelet very well fulfills the condition in (22) and (26). It means a compact support in the time and frequency spaces which satisfies the maximum correlation between the signal and the mother wavelet.

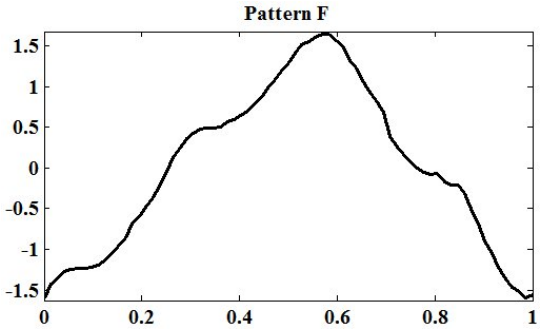

Fig. 5: Gait (walking) pattern

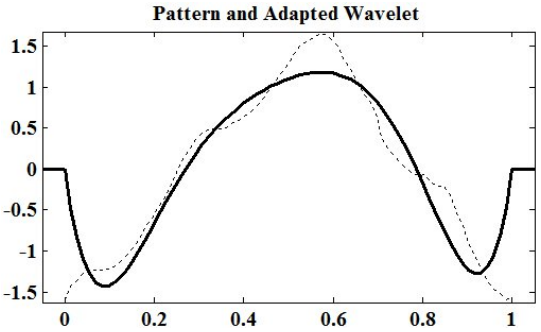

Fig. 6: Adapted mother wavelet

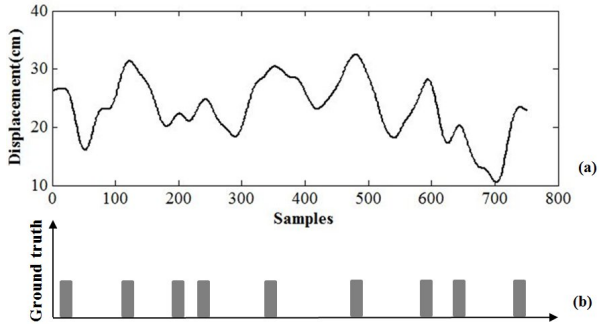

Fig. 7: Original signal (a) and generated ground truth (b)

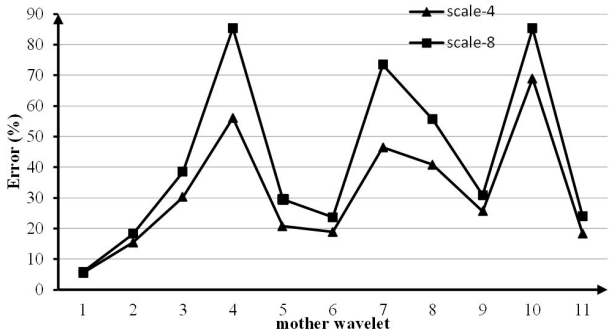

Fig. 8: Detection error (%) for the scale variation

5. RESULTS AND DISCUSSION

Different tests were carried out to evaluate the performance of the adapted wavelet under various conditions, with the presence of noise and scale variation, and to compare with other mother wavelets. A set of mother wavelets (Daubechies: db3, db6, db10, Biorthogonal: bio2.4, Coiflet: coif1, coif5, symlet: sym2, sym8, Marlet and Mexican Hat) with the similar shape and form was selected for this purpose. Horizontal axis in Fig. 8 and 9 refers to the member of this set in accordance with the order mentioned above, staring with db3(2) and end to Mexican Hat (11). Number 1 refers to the proposed mother wavelet, "Wave1".

Moreover, a ground truth signal (Fig. 7.b) was generated to measure the error under different conditions. The pattern is located in a part of the signal where correlation between the scaled mother wavelet (shown in Fig. 6) and the signal holds the highest value comparing to the neighboring values within an interval.

These points in Fig. 7.b are highlighted with vertical gray rods. MRA uses the selected mother wavelet to detect the pattern location. Accumulative difference between results and ground truth forms the error (%). Pattern scaled by 4 and 8, were selected to detect in the original signal (Fig. 7.a). The error of the pattern detection by different mother wavelets were calculated and depicted in Fig. 8. As seen, adapted mother wavelet has the minimum error (5%) while other mother wavelets generated errors from 20% to 85%. The same thing is true when the signal is processed with the presence of noise (Fig. 9). With the presence of Gaussian noise (50% of signal amplitude), the proposed mother wavelet still can detect the position of the pattern with minimum error (8%) while the error for other mother wavelets reaches to up 60%. This shows other unmatched mother wavelets are quite unreliable for this application and adapted wavelet ("Wave1") works with high precision. Besides, the error of the process with the presence of Gaussian noise will yield almost 3 times more error comparing to that of noise-free signal. MRA of walking signal with the presence of noise generate more error than scale variation. It means when the signal has less noise the proposed method can cope with scale variation very successfully. In practice 95% of gaits were analyzed and detected successfully. However, practical implementation shows this method is very bulky for real-time process and need to be processed in parallel stream by GPU or FPGA. The alternative solution is puting physical restrictions which increases the precision up to 100%.

6. CONCLUSION

A practical electro-optic TOF setup for capturing IR image and extracting gait (walking) signal were explained. Then a wavelet adapted from gait pattern and used by multi-resolution analysis was presented to overcome scale variation problems. The result shows 95% of precision is granted for detecting the accurate position of the gait pattern while processing with the proposed mother wavelet creates only 2% error under the scale variation (going from scale 4 to 8). The

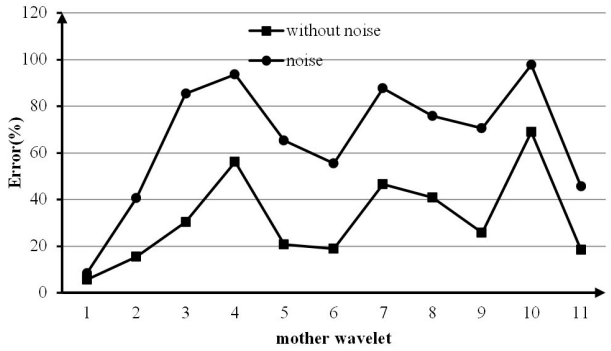

Fig. 9: Error for the noisy and noiseless signals

proposed wavelet also works perfectly with the presence of intensive noise (up 50% of signal amplitude). Processing of noisy signal yield 93% of precision which is significant progress considering the complexity of the real environment.

7. ACKNOWLEDGEMENTS

This work has been founded by the French project FUI Callisto.

8. REFERENCES

[1] Ingrid Daubechies, "Ten lectures on wavelets. society for industrial and applied mathematics, 1992," *Rulgers University and AT&T Bell Laboratories*, vol. 1, pp. 1–36, 2009.

[2] Amit Kumar Ahuja and Ram Chakka, "Symlet2 based wavelet filter bank for uncorrelated digital signal recovery: Some advantages over matched filter," in *Global Trends in Computing and Communication Systems*, pp. 782–791. Springer, 2012.

[3] Ingrid Daubechies, "Orthonormal bases of compactly supported wavelets," *Communications on pure and applied mathematics*, vol. 41, no. 7, pp. 909–996, 1988.

[4] Ahmed H. Tewfik, Deepen Sinha, and Paul Jorgensen, "On the optimal choice of a wavelet for signal representation," *Information Theory, IEEE Transactions on*, vol. 38, no. 2, pp. 747–765, 1992.

[5] Stephane G Mallat and Zhifeng Zhang, "Matching pursuits with time-frequency dictionaries," *Signal Processing, IEEE Transactions on*, vol. 41, no. 12, pp. 3397–3415, 1993.

[6] Akram Aldroubi and Michael Unser, "Families of multiresolution and wavelet spaces with optimal properties," *Numerical Functional Analysis and Optimization*, vol. 14, no. 5-6, pp. 417–446, 1993.

[7] Gianfranco Burzio and Giulio Vivo, "Automotive vision systems," in *Advanced Video-Based Surveillance Systems*, pp. 192–202. Springer, 1999.

[8] Nicholas Peña Ortiz, David Scarlatti, David Esteban, and Pablo Soriano Tapia, "Gesture-based human machine interface," Dec. 14 2011, EP Patent 2,395,413.

[9] David Tolliver and Robert T Collins, "Gait shape estimation for identification," in *Audio-and Video-Based Biometric Person Authentication*. Springer, 2003, pp. 734–742.

[10] Sohail Nadimi and Bir Bhanu, "Physical models for moving shadow and object detection in video," *Pattern Analysis and Machine Intelligence, IEEE Transactions on*, vol. 26, no. 8, pp. 1079–1087, 2004.

[11] Johannes Preis, Moritz Kessel, Martin Werner, and Claudia Linnhoff-Popien, "Gait recognition with kinect," in *1st International Workshop on Kinect in Pervasive Computing*, 2012.

[12] Erik E Stone and Marjorie Skubic, "Passive in-home measurement of stride-to-stride gait variability comparing vision and kinect sensing," in *Engineering in Medicine and Biology Society, EMBC, 2011 Annual International Conference of the IEEE*. IEEE, 2011, pp. 6491–6494.

[13] Erik Stone and Marjorie Skubic, "Evaluation of an inexpensive depth camera for in-home gait assessment," *Journal of Ambient Intelligence and Smart Environments*, vol. 3, no. 4, pp. 349–361, 2011.

[14] Yumi Iwashita, Koji Uchino, and Ryo Kurazume, "Gait-based person identification robust to changes in appearance," *Sensors*, vol. 13, no. 6, pp. 7884–7901, 2013.

[15] Cyrus Bamji and Edoardo Charbon, "Systems for cmos-compatible three-dimensional image sensing using quantum efficiency modulation," June 17 2003, US Patent 6,580,496.

[16] Mohamed Rizon, Yazid Haniza, Saad Puteh, Ali Yeon, Md Shakaff, Masanori Sugisaka, Yaacob Sazali, and M Karthigayan, "Object detection using circular hough transform," *American Journal of Applied Sciences*, vol. 2, no. 12, pp. 1606–1609, 2005.

[17] John J Benedetto and Shidong Li, "The theory of multiresolution analysis frames and applications to filter banks," *Applied and Computational Harmonic Analysis*, vol. 5, no. 4, pp. 389–427, 1998.

[18] Harold Szu, Yunlong Sheng, and Jing Chen, "Wavelet transform as a bank of the matched filters," *Applied optics*, vol. 31, no. 17, pp. 3267–3277, 1992.